HHS Public Access

Author manuscript

Cancer Res. Author manuscript; available in PMC 2022 October 15.

Published in final edited form as:

Cancer Res. 2022 April 15; 82(8): 1589–1602. doi:10.1158/0008-5472.CAN-22-0059.

Combinatorial inactivation of tumor suppressors efficiently initiates lung adenocarcinoma with therapeutic vulnerabilities

Maryam Yousefi[1,8,*], **Gábor Boross**[4,8], **Carly Weiss**[4], **Christopher W. Murray**[2], **Jess D. Hebert**[1], **Hongchen Cai**[1], **Emily L. Ashkin**[2], **Saswati Karmakar**[1], **Laura Andrejka**[1], **Leo Chen**[1], **Minwei Wang**[1], **Min K. Tsai**[1], **Wen-Yang Lin**[1], **Chuan Li**[4], **Pegah Yakhchalian**[7], **Caterina I. Colón**[2], **Su-Kit Chew**[5,6], **Pauline Chu**[3], **Charles Swanton**[5,6], **Christian A. Kunder**[3], **Dmitri A. Petrov**[2,4], **Monte M. Winslow**[1,2,3,*]

[1]Department of Genetics, Stanford University School of Medicine, Stanford, CA, USA

[2]Cancer Biology Program, Stanford University School of Medicine, Stanford, CA, USA

[3]Department of Pathology, Stanford University School of Medicine, Stanford, CA, USA

[4]Department of Biology, Stanford University, Stanford, CA, USA

[5]Cancer Evolution and Genome Instability Laboratory, University College London Cancer Institute, London, UK

[6]Cancer Evolution and Genome Instability Laboratory, The Francis Crick Institute, London, UK

[7]Department of Medicine, David Geffen School of Medicine at University of California, Los Angeles, Los Angeles, CA, USA

[8]These authors contributed equally

Abstract

Lung cancer is the leading cause of cancer death worldwide, with lung adenocarcinoma being the most common subtype. Many oncogenes and tumor suppressor genes are altered in this cancer type, and the discovery of oncogene mutations has led to the development of targeted therapies that have improved clinical outcomes. However, a large fraction of lung adenocarcinomas lacks mutations in known oncogenes, and the genesis and treatment of these oncogene-negative tumors remain enigmatic. Here, we perform iterative in vivo functional screens using quantitative autochthonous mouse model systems to uncover the genetic and biochemical changes that enable efficient lung tumor initiation in the absence of oncogene alterations. Generation of hundreds of diverse combinations of tumor suppressor alterations demonstrates that inactivation of suppressors of the RAS and PI3K pathways drives the development of oncogene-negative lung adenocarcinoma. Human genomic data and histology identified RAS/MAPK and PI3K pathway activation as a common event in oncogene-negative human lung adenocarcinomas. These Onc-negative$^{RAS/PI3K}$ tumors and related cell lines are vulnerable to pharmacological inhibition of

[*]Corresponding authors: Monte M. Winslow, Stanford University School of Medicine | 279 Campus Drive, Beckman Center B256, Stanford, CA 94305. Phone: 650-725-8696 | Fax: 650-725-1534 mwinslow@stanford.edu; Maryam Yousefi, Stanford University School of Medicine | 279 Campus Drive, Beckman Center B261, Stanford, CA 94305. Phone: (650) 725-2182| yousefi@stanford.edu.

these signaling axes. These results transform our understanding of this prevalent yet understudied subtype of lung adenocarcinoma.

INTRODUCTION

Lung cancer is the leading cause of cancer death (1). Lung adenocarcinoma, the most prevalent subtype of lung cancer, has frequent alterations in receptor tyrosine kinase and RAS/RAF pathway oncogenes, including mutations in *EGFR* and *KRAS* (2). The identification of driver oncogenes has enabled a shift from toxic chemotherapies to less toxic and more effective therapies that often target the oncogenes (3). However, approximately 30 percent of lung adenocarcinomas are thought to lack a driving oncogene (4–6). Consequently, developing targeted therapies for these tumors remains a major unmet challenge for precision thoracic oncology.

Extensive genomic and transcriptomic studies suggest that neither technical reasons nor the presence of novel oncogenes likely explains this large and clinically significant population of lung cancer patients(1, 2, 4–10). Thus, despite the diagnosis of more than 150,000 patients per year with oncogene-negative lung adenocarcinomas worldwide, the genetic events and biochemical pathway changes that drive the initiation and growth of these tumors remain almost entirely unknown.

Oncogenes and tumor suppressor genes are parts of signaling networks that generate and sustain the biochemical changes that drive tumor initiation and growth (11–13). Combinatorial alterations in tumor suppressor genes could co-operate to activate pathways driving oncogene-negative lung tumors. Human lung adenocarcinoma have complex patterns of mutations across many putative tumor suppressor genes (4). However, the ability to predict which combinations of genomic alterations drive cancer in the absence of oncogene activation based on human genomic data alone remains challenging. While human genomic data can predict combinations of genomic mutations as likely cancer drivers when the mutations co-occur at very high frequencies (14–17), identifying pathogenic combinations of less frequently mutated genes poses a nearly insurmountable statistical challenge. Furthermore, the large numbers of mutations in lung cancers, non-genomic mechanism that often inactivate tumor suppressor genes, and generation of similar biochemical effects through inactivation of different genes further reduce the ability of human cancer genomic studies to identify combinatorial alterations that activate driver pathways in lung cancer (18–21).

Functional genomic studies within autochthonous cancer models can help identify the pathways involved in tumorigenesis *in vivo* (22). Here, we leveraged quantitative mouse model systems to assess the ability of hundreds of combinatorial alterations of tumor suppressor genes, acting across many different signaling pathways, to generate oncogene-negative lung adenocarcinomas *in vivo*. We uncover pathway-level changes that drive lung cancer in the absence of oncogene mutations, translate these findings to human oncogene-negative lung adenocarcinoma, and leverage these results to identify therapeutic vulnerabilities.

MATERIALS AND METHODS

Analysis of human lung adenocarcinoma datasets

Somatic mutation data (SNPs and indels, including silent mutations), TCGA-LUAD clinical and exposure data, and GISTIC2 thresholded copy number variation for 513 TCGA lung adenocarcinoma (LUAD) tumors were downloaded from https://tcga.xenahubs.net/download/mc3/LUAD_mc3.txt.gz, https://portal.gdc.cancer.gov/projects/TCGA-LUAD, https://tcga.xenahubs.net/download/TCGA.LUAD.sampleMap/LUAD_clinicalMatrix, https://tcga.xenahubs.net/download/TCGA.LUAD.sampleMap/Gistic2_CopyNumber_Gistic2_all_thresholded.by_genes.gz.

Amplifications were defined as “2” and deletions as “−2”. Genes with conflicting CNV values within a single tumor were ignored. Fusion data were obtained from (23). Fusion and CNV data were filtered to include only data from the 513 samples within the somatic mutation set. Duplicate fusions were collapsed into single fusions. MET-exon skipping data were taken from (24). Curated survival data from (25) were downloaded from https://tcga.xenahubs.net/download/survival/LUAD_survival.txt.gz.

Somatic mutations, copy number alteration (CNA) data, fusion data, panel information (genomic_information.txt), and clinical data (both sample- and patient-level) from AACR Project GENIE v8 were downloaded from https://www.synapse.org/#!Synapse:syn22228642 (25). Data were filtered to only include LUAD tumors. A single tumor was kept for patients with multiple different tumor samples, with priority for earlier sequenced samples and those from primary tumors. If tumor samples appeared identical within the clinical meta-data, the related patient data were excluded. Criteria for determining the fraction of lung adenocarcinomas without known oncogenic drivers, classification of mutations and tumors, and gene and pathway alteration co-occurrences (Supplemental Methods).

Animal Studies

The use of mice for the current study has been approved by Institutional Animal Care and Use Committee at Stanford University, protocol number 26696. *Kras*$^{LSL\text{-}G12D/+}$ (Jax # 008179 (*K*)), *R26*$^{LSL\text{-}tdTomato}$(*ai9*) (Jax # 007909 (*T*)), and *H11*$^{LSL\text{-}Cas9}$ (Jax # 026816 (*C*)), *Keap1*^{flox}, *Pten* ^{flox} (Jax # 006440), *Lkb1* ^{flox} (Jax # 014143), *Nf1* ^{flox} (Jax # 017640), and *Trp53*^{flox} (Jax # 008462) mice have been previously described (26–33). All mice were on a C57BL/6:129 mixed background except the mice used for generation of oncogene-negative cell lines and some of the *Trp53*$^{flox/flox}$;*TC* mice used for metastasis analysis, which were on a pure C57BL/6 background.

Tumor initiation

Tumors were initiated by intratracheal delivery of pooled or individual Lenti-sgRNA/*Cre* vectors. Tumors were initiated with the indicated titers and allowed to develop tumors for 3 to 12 months after viral delivery, as indicated in each figure (see Supplementary Methods).

Tumor barcode sequencing and analysis

For DNA extraction from single dissected tumors to generate libraries for Tuba-seq, targeted sequencing of selected oncogenes, and whole-exome sequencing, we used Qiagen AllPrep DNA/RNA Micro kit. For Tuba-seq on bulk lungs, genomic DNA was isolated from bulk tumor-bearing lung tissue from each mouse as previously described (34). Q5 High-Fidelity 2x Master Mix (New England Biolabs, M0494X) was used to amplify the sgID-BC region from 50 ng of DNA from dissected tumors or 32 μg of bulk lung genomic DNA. Unique dual-indexed primers were used for each sample (35). The PCR products were purified with Agencourt AMPure XP beads (Beckman Coulter, A63881) using a double size selection protocol. The libraries were pooled based on lung weights to ensure even reading depth, and sequenced (read length 2×150bp) on the Illumina HiSeq 2500 or NextSeq 500 platform (Admera Health Biopharma Services). Tuba-seq analysis of tumor barcode reads was performed as previously described (34, 36) (Supplemental Methods. We used several metrics of tumor number, burden, and size (see Supplemental Figure 4 in (35) and Supplemental Methods).

Multiple transductions

A fraction of lung tumors initiated with Lenti-sg*RNA*/*Cre* vectors contained multiple barcoded Lenti-sgRNA/Cre vectors. If multiple barcodes (sgID-BCs) have unexpectedly similar read counts, we suspect transduction of the initial cell with multiple Lenti-sg*RNA/Cre* vectors. To capitalize on these multiple transductions as a way to find higher-order interactions between tumor suppressor genes, we identify the combinations of sgRNA that appear to cooperate as potent drivers of tumor growth. We developed methods to identify tumors with likely multiple transductions (*i.e.*, those tumors with complex genotypes with multiple tumor suppressor genes inactivated). For each sgID-BC, we consider sgID-BCs from the same sample with read counts within 10% as possible multiple transduction events. Multiple transductions that lead to synergistic combinatorial tumor suppressor alterations would confer a growth advantage. Thus, synergistic combinatorial alterations of tumor suppressor genes would be expected to be overrepresented among the largest tumors.

To have a dataset with a higher signal-to-noise ratio, we analyzed the largest tumors that were co-infected with up to 6 Lenti-sgRNA/*Cre* vectors. With this method, for each tumor, we assembled a list of genes that were possibly co-mutated. We then ranked all possible combinations of genes by their frequency in the largest tumors. An inherent problem with this analysis is that the genotypes that increase tumor growth will be overrepresented amongst the largest tumors even without multiple transductions and specific synergistic interactions. To account for the different number of tumors with different sgIDs, we performed a permutation test, where we control for the number of tumors of each genotype but randomize the sizes of tumors by randomly matching the genotypes with tumor sizes (10,000 repetitions). Synergistic tumor suppressor combinations will occur at significantly higher than expected frequencies based on this permutation test. Reassuringly, while our analysis resulted in significant enrichment of complex genotypes based on the permutation test, a control analysis performed on smaller tumors within the same mice with high noise to

signal ratio resulted in a loss of statistical significance, this shows that our permutation test controls for the bias of different frequency of sgIDs among the tumors.

Histology and immunohistochemistry

Lung lobes were inflated with 4% formalin and fixed for 24 hours, stored in 70% ethanol, paraffin-embedded, and 4 μm thick sections were used for Hematoxylin and Eosin (H&E) staining and immunohistochemistry (IHC). Primary antibodies were anti-RFP (Rockland, 600-401-379), anti-TTF1(Abcam, ab76013), anti-UCHL1(Sigma, HPA005993), anti-TP63 (Cell Signaling Technology, 13109), anti-phospho-S6 (Cell Signaling Technology, 4858), anti-PTEN (Cell Signaling Technology, 9559), anti-phospho-ERK (Cell Signaling Technology, 4370), anti-phospho-AKT (Thermo Fisher Scientific, 44-621G), and anti-HMHGA2 (Biocheck, 59170AP). IHC was performed using Avidin/Biotin Blocking Kit (Vector Laboratories, SP-2001), Avidin-Biotin Complex kit (Vector Laboratories, PK-4001), and DAB Peroxidase Substrate Kit (Vector Laboratories, SK-4100) following standard protocols.

To quantify the positivity of phospho-ERK and phospho-AKT stained slides, H-scores were calculated using Qupath. The H-score is determined by adding the results of multiplication of the percentage of cells with staining intensity ordinal value (scored from 0 for “no signal” to 3 for “strong signal”) with possible values ranging from 0 to 300 (37). To normalize potential variations between different rounds of immunohistochemistry, one patient sample was included and stained for both pERK and pAKT in all rounds of staining as a control.

Cell Lines

Mouse oncogene-negative cell lines were generated from tumors initiated in *Trp53*$^{flox/flox}$;*TC BL6* mice four months after transduction with Lenti-sg*Nf1*-sg*Rasa1*-sg*Pten*/*Cre*. After dissociation of tumors, cells were cultured in DMEM supplemented with 10% FBS, 1% penicillin/streptomycin (Gibco), and 0.1% Amphotericin (Life Technologies). HC494 and MW389T2 (*Kras*^{G12D} and *Trp53* mutant) lung adenocarcinoma cells were previously generated. Human oncogene-negative cell lines (NCI-H1838, NCI-H1623) and oncogene-positive cell lines (A549, H2009, NCI-H2009, SW1573, HOP62, NCI-H358, NCI-H1792) were purchased from ATCC and cultured in RPMI supplemented with 5%FBS, 1% penicillin/streptomycin (Gibco), and 0.1% Amphotericin (Life Technologies). We performed mycoplasma testing using MycoAlert™ Mycoplasma Detection Kit (Lonza). Cell were maintained at 37°C in a humidified incubator at 5% CO_2. NCI-H1838 and NCI-H1623 cell lines do not have any genomic mutation in components of PI3K pathway. Mutations of these two cell lines in components of RAS pathway are indicated below (extracted from DepMap):

NCI-H1838 mutations in RAS pathway: NF1(p.N184fs) and IQGAP2 (p.P780L)

NCI-H1623 mutations in RAS pathway: RASA1 (p.A47fs), FGFR2 (p.A355S), and ERF (p.G255C)

Clonogenic, apoptosis, and proliferation assays

For clonogenic assays, mouse cells were seeded in triplicate into 24-well plates (4000 cells per well) and allowed to adhere overnight in regular growth media. Cells were then cultured in the absence or presence of the drug as indicated on each figure panel in complete media for 4 days. Growth media with or without drugs was replaced every 2 days. The remaining cells were stained with 0.5% crystal violet in 20% methanol and photographed using a digital scanner. Relative growth was quantified by densitometry after extracting crystal violet from the stained cells using 100% methanol (38).

Clonogenic assay of human oncogene-negative lung adenocarcinoma cell lines was done in spheroids (39). 400–5000 cells/well were seeded in round bottom ultra-low attachment 96-well plates (Corning) in growth media and incubated for 72 hours at 37°C in 5% CO2. Spheroid formation was confirmed visually, and spheroids were treated in triplicate with dilutions of RMC-4550 and capivasertib in complete growth media. Following drug exposure for five days, cell viability in spheroids was determined using the CellTiter-Glo 3D assay kit (Promega), following the manufacturer's instructions. Data was normalized to DMSO values.

Drug synergy was analyzed using SynergyFinder (https://synergyfinder.fimm.fi) web application (40). The degree of combination synergy, or antagonism, was quantified by comparing the observed drug combination response against the expected response, calculated using Loewe's model that assumes no interaction between drugs (41).

For apoptosis and proliferation assays, 3×10^5 cells were seeded into 6-well plates, allowed to adhere overnight in regular growth media, and cultured in the presence or absence of 10 μM of Capivasertib, RMC-4550, or a combination of both drugs. After 24 hours, apoptosis and cell proliferation were determined through staining with Fixable Viability Dye eFluor™ 450 (Thermo Fisher Scientific, 65-0863-14), cleaved caspase 3 Antibody (Cell Signaling Technology, 9669), and Click-iT™ EdU Alexa Fluor™ 647 Flow Cytometry Assay Kit (Thermo Fisher Scientific, C-10424) according to the manufacturer's instructions. Data were acquired using a BD LSR II Flow Cytometer. All experiments were performed independently two times on 3 different cell lines.

In vivo drug response studies

For drug efficacy studies in autochthonous mouse models, *TC* mice (8–12 weeks old) were divided into 4 groups randomly 3.5 months after tumour initiation. They received the vehicle, capivasertib (100 mg/kg, MedChemExpress), RMC-4550 (30 mg/kg, MedChemExpress), or a combination of both dissolved in 10% DMSO, 40% PEG, 5% Tween 80, and 45% PBS through oral gavage. Mice were treated daily for eight days, and the treatment was stopped for two days for recovery, and continued for two more days before the tissue harvest. The last two doses of combination therapy were half of the initial doses.

Cell line-derived allografts were generated through subcutaneous injection of 300,000 of MY-C3 (*Nf1*, *Rasa1*, *Pten*, and *Trp53* mutant) oncogene-negative mouse cell line in 200 μl of PBS in male (6–8 week old) BL6 mice (two tumors per mouse). Once tumors reached an

average size of ~100 mm^3 administration of RMC-4550 (30 mg/kg, MedChemExpress) and capivasertib (100 mg/kg, MedChemExpress) (5 days on, 2 days off) for 17 days.

Tumor dissociation, cell sorting, and RNA-sequencing

Primary tumors were dissociated using collagenase IV, dispase, and trypsin at 37 °C for 30 min. After dissociation, the samples remained continually on ice, were in contact with ice-cold solutions, and were in the presence of 2 mM EDTA and 1 U/ml DNase to prevent aggregation. Cells were stained with antibodies to CD45 (BioLegened, 103112), CD31 (BioLegend, 303116), F4/80 (BioLegend, 123116), and Ter119 (BioLegend, 116212) to exclude hematopoietic and endothelial cells (lineage-positive (Lin^+) cells). DAPI was used to exclude dead cells. FACS Aria sorters (BD Biosciences) were used for cell sorting.

RNA was purified using RNA/DNA All Prep kit (Qiagen, 80284). RNA quality of each tumor sample was assessed using the RNA6000 PicoAssay for the Agilent 2100 Bioanalyzer as per the manufacturer's recommendation. 4.4 ng total RNA per sample was used for cDNA synthesis and library preparation using Trio RNA-Seq, Mouse rRNA kit (Tecan, 0507-32), according to the manufacturer's instructions. The purified cDNA library products were evaluated using the Agilent bioanalyzer and sequenced on NextSeq High Output 1×75 (Admera Health Biopharma Services).

Analysis of mouse model-derived RNA-seq datasets

Paired-end RNA-seq reads were aligned to the mm10 mouse genome using STAR (v2.6.1d) 2-pass mapping and estimates of transcript abundance were obtained using RSEM (v1.2.30) (42, 43). The differentially expressed genes between different tumor genotypes and treatment groups were called by DESeq2 using transcript abundance estimates via tximport (44, 45). The DESeq2-calculated fold changes were used to generate ranked gene lists for input into GSEA (46).

The upregulated genes with absolute log2 fold change greater than 1 and a false discovery rate less than 0.05 in the comparison of *Nf1*, *Rasa1*, and *Pten* mutant oncogene-negative tumors with $Kras^{G12D}$-driven tumors (*KTC*+sg*Inert* and *KTC*+sg*Pten)* were compiled into a signature reflecting the oncogene-negative adenocarcinoma state. This gene signature was utilized in the analysis of human oncogene-positive and oncogene-negative tumors. Scaled estimates of transcript abundance for TCGA LUAD samples were obtained from the GDC data portal (gdc-portal.nci.nih.gov). Each expression profile was then scored on the basis of the mouse-derived gene signature using single-sample GSEA within the Gene Set Variation Analysis (GSVA) package (47).

Statistical analysis

The statistical analyses were performed using R, Python, and Prism software environments. For all bar plots showing relative tumor size, tumor number, tumor burden and frequency, p-values and 95% confidence intervals (represented by whiskers) were calculated using bootstrap resampling (10000 repetitions, see Supplemental Methods). For all box plots, center lines represent the median, box limits represent the interquartile range. For all strip plots, lines represent the mean. For all box plots and strip plots, statistical significance was

calculated by the Wilcoxon rank sum test. For “frequency in large tumors”, a permutation test was used to calculate p-values (see Supplemental Methods). Two-sided Fisher’s exact test was used to determine statistical significance of alteration frequencies in tumor suppressor genes and oncogenic pathways. Survival curves were compared with the log-rank test. For H-scores, center lines represent the mean, and the p-values are calculated using Mann-Whitney test in Prism.

Data availability statement

Tuba-seq barcode sequencing and RNA-seq data have been deposited in NCBI’s Gene Expression Omnibus (https://www.ncbi.nlm.nih.gov/geo/) (GSE174393). Whole exome sequencing data generated are publicly available in SRA-NCBI (www.ncbi.nlm.nih.gov/sra) (PRJNA769722).

RESULTS

A large fraction of human lung adenocarcinomas lack oncogene mutations

To better understand the genomics of lung adenocarcinomas that lack oncogene mutations, we analyzed data from The Cancer Genome Atlas (TCGA) and AACR Genomics Evidence Neoplasia Information Exchange (GENIE) (48, 49). We classified tumors as oncogene-positive if they had high-confidence oncogenic alterations in previously described proto-oncogenes, oncogene-indeterminate if they had alterations of unknown significance in known proto-oncogenes, and oncogene-negative if they had no alterations in known proto-oncogenes (Methods). Consistent with previous publications, we found that 17–18% of lung adenocarcinomas were oncogene-negative (Figure 1a and S1a) (50–52). Additionally, 15–27% of lung adenocarcinomas were oncogene-indeterminate and thus 32–45% of lung adenocarcinomas lack known oncogene mutations. Patients with oncogene-negative, oncogene-indeterminate, and oncogene-positive lung adenocarcinomas have broadly similar mutational burden and clinical characteristics (Figure S1b–e).

Combinatorial tumor suppressor gene inactivation enables lung tumor development

To determine whether combinatorial tumor suppressor gene inactivation can drive lung tumor initiation in the absence of oncogene activation, we coupled Cre/*loxP*-based genetically engineered mouse models and somatic CRISPR/Cas9-based genome editing with tumor barcoding and high-throughput barcode sequencing (Tuba-seq) (29, 30, 34–36, 53, 54). We used Cre*/loxP* to inactivate each of five “core” tumor suppressor genes (*Trp53*, *Lkb1/Stk11*, *Keap1*, *Nf1*, and *Pten)*. These genes are within diverse pathways and are frequently inactivated in human lung cancers, including oncogene-negative lung adenocarcinomas (Figure S2a–b). We used CRISPR/Cas9 to coincidentally inactivate panels of additional tumor suppressor genes in lung epithelial cells in mice with floxed alleles of each of the “core” tumor suppressors, a Cre-reporter allele ($R26^{LSL\text{-}Tom}$ (*T*) (29)), and a Cre-regulated *Cas9* allele ($H11^{LSL\text{-}Cas9}$ (*C*) (30)).

We transduced $Nf1^{f/f}$;*TC,* $Pten^{f/f}$;*TC,* $Trp53^{f/f}$;*TC,* $Lkb1^{f/f}$;*TC,* $Keap1^{f/f}$;*TC, TC*, and *T* mice with two pools of barcoded Lenti-sgRNA*/Cre* vectors that target ~50 putative tumor suppressor genes that we previously investigated in $KRAS^{G12D}$-driven lung tumors

(Lenti-sg*TS*15/*Cre* and Lenti-sg*TS*102/*Cre*) (Figure 1b, S2c–d, S3a, and Table S1) (34–36). The mutation frequency of these genes varied, and mutations in some were enriched in oncogene-negative human lung adenocarcinomas (Table S1) (Figure S2c–d). The combination of Cre/*LoxP* and CRISPR/Cas9-based genome editing should generate hundreds of combinations of genomic alterations in lung epithelial cells. We previously found that a small percent of lung tumors initiated with Lenti-sgRNA/*Cre* vectors in other lung cancer models contained multiple sgRNAs, consistent with the transduction of the initial cell with multiple Lenti-sgRNA/*Cre* vectors (34, 36). Thus, we used a high titer of the Lenti-sgRNA/*Cre* pools in these experiments to increases the likelihood of finding higher-order genetic interactions that drive tumorigenesis.

One year after transduction with the Lenti-sg*RNA/Cre* pools, *Nf1*$^{f/f}$;*TC*, *Pten*$^{f/f}$;*TC*, and *Trp53*$^{f/f}$;*TC* mice developed a modest number of tumors (defined as Tomato^{positive} expansion >0.5 mm in diameter) (Figure 1c–d, S3b–c). Interestingly, *Nf1*$^{f/f}$;*TC*, *Pten*$^{f/f}$;*TC*, and *Trp53*$^{f/f}$;*TC*, and *TC* mice transduced with the larger Lenti-sg*TS102/Cre* pool developed many more tumors than those transduced with the Lenti-sg*TS15/Cre* pool. These tumors were positive for TTF1/NKX2-1, a marker for lung adenocarcinoma, and negative for P63 and UCHL1, markers for squamous cell and small cell lung cancer, respectively (Figure 1e).

To determine whether these tumors contained spontaneous oncogene mutations, we sequenced 10 genomic regions in *Kras, Braf*, *Nras*, and *Egfr* (Figure S3d, Table S2, and Methods) (28, 53, 55–62). Across 29 samples, we detected only one oncogene mutation (a *Kras*^{G12V} mutation in a tumor from a *Pten*$^{f/f}$;*TC* mouse). Thus, the majority of these tumors arose in the absence of hotspot mutations in these proto-oncogenes. This suggests that the inactivation of combinations of specific tumor suppressor genes in *Nf1*$^{f/f}$;*TC*, *Pten*$^{f/f}$;*TC*, and *Trp53*$^{f/f}$;*TC* mice drives the development of lung cancer *in vivo*. Notably, the overall low number of tumors indicates that inactivation of the “core” tumor suppressor genes alone, and most combinations of tumor suppressor genes tested, are insufficient to generate lung tumors.

Identification of top candidate tumor suppressor genes involved in oncogene-negative lung tumor formation

The Lenti-sgRNA/Cre vectors contain two-component barcodes in which an sgID identifies the sgRNA and a random barcode (BC) uniquely tags each clonal tumor. Thus, high throughput sequencing of the sgID-BC region can identify the sgRNA(s) present in each tumor and quantify the number of cancer cells in each tumor (Figure 1b). To determine which sgRNAs were present in the largest tumors, we PCR-amplified the sgID-BC region from genomic DNA from dissected tumors and performed high-throughput sgID-BC sequencing. Most large tumors contained multiple Lenti-sgRNA/*Cre* vectors therefore, we calculated the statistical enrichment of each sgRNA based on their relative representation in the dissected tumors (Figure 1f and S4, see Methods).

To further quantify the impact of inactivating each tumor suppressor gene on clonal expansion of lung epithelial cells, we performed tumor barcode sequencing (Tuba-seq) on bulk DNA from one lung lobe from each *Nf1*$^{f/f}$;*TC*, *Pten*$^{f/f}$;*TC, Trp53*$^{f/f}$;*TC*, and *TC* mouse (Figure 1c). Analysis of the number of cells in clonal expansions further nominated tumor

suppressor genes that may contribute to tumor initiation and growth (Figure 1f, and S5). Based on these two analyses, we selected 13 genes for further analysis (Figure 1f). The potential importance of these tumor suppressor genes was often supported by both sgRNAs targeting each gene, consistent with on-target effects (Figure 1f and S4–5).

Inactivation of candidate tumor suppressors efficiently generates lung tumors

To determine whether inactivation of candidate tumor suppressor genes can initiate oncogene-negative tumors, we generated a pool of Lenti-sgRNA*/Cre* vectors targeting each of these tumor suppressor genes (Lenti-sg*TS14/Cre* pool; Figure 2a). We targeted each gene with the sgRNA that had the most significant effect on tumor growth and used five times higher titer of each lentiviral vector per mouse than we used in Lenti-sg*TS102/Cre* pool, thus increasing the potential for the transduction of the initial cell with multiple Lenti-sgRNA*/Cre* vectors.

We initiated tumors with Lenti-sg*TS14/Cre* in $Nf1^{f/f}$;*TC*, $Pten^{f/f}$;*TC, Trp53*$^{f/f}$;*TC, TC*, and $Kras^{LSL\text{-}G12D}$;*T* (*KT*) mice. Less than four months after tumor initiation, several $Nf1^{f/f}$;*TC* and $Pten^{f/f}$;*TC* mice showed signs of extensive tumor burden. These mice developed many more tumors than mice of the same genotypes one year after transduction with the Lenti-sg*TS102/Cre* (compare Figure 2b–c with Figure 1c–d). We performed Tuba-seq on DNA from tumor-bearing lungs to determine the number and size of tumors with each barcoded Lenti-sgRNA/*Cre* vector. Inactivation of *Nf1, Rasa1*, and *Pten* most dramatically increased tumor size and/or tumor number across all mouse genotypes (Figure 2d–e, S6a–b, and Methods). Inactivation of several other tumor suppressor genes less dramatically but significantly increased tumor size and/or tumor number in a genotype-specific manner, suggests that additional molecular pathways may also lead to early epithelial expansions.

The largest tumors in $Nf1^{f/f}$;*TC*, $Pten^{f/f}$;*TC, Trp53*$^{f/f}$;*TC*, and *TC* mice were frequently generated through the inactivation of multiple tumor suppressor genes. Vectors targeting *Nf1*, *Rasa1*, and/or *Pten* were often present in the largest tumors, and the coincident targeting of *Nf1*, *Rasa1*, and *Pten* was the most frequent combination (Figure 2f–g, S6c–h). To gain greater insight into the contribution of *Nf1*, *Rasa1*, and *Pten* inactivation to the generation of oncogene-negative tumors, we transduced $Nf1^{f/f}$;*TC*, $Pten^{f/f}$;*TC,Trp53*$^{f/f}$;*TC, TC*, and *KT* mice with a pool of Lenti-sgRNA*/Cre* vectors that lacked the vectors targeting *Nf1*, *Rasa1*, and *Pten* (*Lenti-sgTS11/Cre)* (Figure S7a). Approximately four months after transduction, these mice had many fewer tumors than mice transduced with Lenti-*sgTS14/Cre* pool (Figure S7b–c). Tuba-seq analysis confirmed a dramatic decrease in tumor burden relative to mice that received the Lenti-sg*TS14/Cre pool* (Figure 2h). Thus, the inactivation of *Nf1, Rasa1*, and *Pten* emerged as the most important contributors to the generation of oncogene-negative lung tumors.

Extensive experiments generating single and pairwise inactivation of tumor suppressor genes in individual mice led to the development of very few tumors even after long periods of time (Figure S8–9). Thus, single and pairwise tumor suppressor gene inactivation is rarely sufficient to generate lung tumors and combinatorial inactivation of three or more tumor suppressor genes increases the efficiency of tumor development and/or accelerates the growth of oncogene-negative lung tumors.

Combinatorial inactivation of *Nf1, Rasa1*, and *Pten* drives lung adenocarcinoma development comparably to oncogenic KRAS

To investigate the contribution of *Nf1*, *Rasa1*, and *Pten*, we transduced *TC* and *Trp53*$^{f/f}$;*TC* mice with a pool of eight lentiviral vectors that would inactivate *Nf1, Rasa1*, and *Pten* individually, in pairwise combinations, and all three simultaneously (Lenti-sg*TS*$^{Triple\text{-}pool}$/*Cre*, Figure 3a). Three months after tumor initiation, *TC* mice had hundreds of large adenomas and adenocarcinomas (Figure 3b–d and Figure S10a–e). Tuba-seq analysis showed that most of the tumor burden arose as a consequence of concomitant inactivation of all three tumor suppressors (Figure 3e and S8). Additional inactivation of *Trp53* in *Trp53*$^{f/f}$;*TC* mice did not increase tumor initiation suggesting that *Trp53* is not a major suppressor of oncogene-negative lung adenocarcinoma development at these early stages (Figure 3b–f and Figure S10a–f). Finally, to compare the tumor initiation potential of combinatorial *Nf1*, *Rasa1*, and *Pten* inactivation with that of a known oncogene, we transduced *Kras*$^{LSL\text{-}G12D}$;*T* mice (which lack Cas9) with Lenti-sg*TS*$^{Triple\text{-}pool}$/*Cre* (Figure 3a). Strikingly, coincident inactivation of *Nf1, Rasa1*, and *Pten* in *TC* and *Trp53*$^{f/f}$;*TC* mice was nearly as potent as oncogenic KRAS^{G12D} in driving lung tumor initiation *in vivo* (Figure 3f, Figure S10g, and Methods).

Finally, we initiated tumors in *TC* and *Trp53*$^{f/f}$;*TC* mice using only the lentiviral vector that targets all three genes (Lenti-sg*Nf1*-sg*Rasa1*-sg*Pten*/*Cre*) (Figure S11a). After only three months, these mice developed very large numbers of lung adenomas and adenocarcinomas (Figure S11b–e). We confirmed the inactivation of *Nf1*, *Rasa1*, and *Pten* in these tumors and whole-exome sequencing uncovered no putative oncogene mutations and only a few putative tumor suppressor mutations (Figure S11f and Table S3). Interestingly, at later time points after initiation, tumors in *Trp53*$^{f/f}$;*TC* mice progressed to an invasive NKX2–1^{negative} HMGA2^{positive} state and metastasized to other organs (Figure S12) (63).

Oncogene-negative murine lung adenocarcinomas have activated RAS and PI3K pathways

NF1 and RASA1 are negative regulators of RAS, while PTEN is a negative regulator of the PI3K-AKT pathway. Therefore, we investigated the impact of inactivating these tumor suppressor genes on RAS and PI3K pathway activation by immunohistochemistry and RNA-seq on FACS-isolated Tomato^{positive} cancer cells. We generated autochthonous tumors in which *Nf1*, *Rasa1*, and *Pten* were inactivated (*TC* mice with Lenti-sg*Nf1*-sg*Rasa1*-sg*Pten*/*Cre*; Nf1/Rasa1/Pten tumors), KRAS^{G12D} was expressed (*KT;H11*$^{LSL\text{-}Cas9}$ mice with Lenti-sg*Inert*/*Cre*; Kras tumors), or KRAS^{G12D} was expressed and *Pten* was inactivated (*KT;H11*$^{LSL\text{-}Cas9}$ mice with Lenti-sg*Pten*/*Cre*; Kras/Pten tumors) (Figure S13a). Nf1/Rasa1/Pten tumors had positive staining for pERK (indicative of RAS pathway activation) and pAKT (indicative of PI3K pathway activation) (Figure 4a). Compared with Kras/Pten tumors, the average pERK staining in Nf1/Rasa1/Pten tumors was less intense and pAKT staining was similar (Figure 4b–c). Single-sample gene set variation analysis (ssGSVA) on our RNA-seq data confirmed that Nf1/Rasa1/Pten tumors had lower RAS pathway gene signature scores than Kras/Pten tumors (Figure S13b) (64, 65). PI3K-AKT pathway gene signature scores were similar in Nf1/Rasa1/Pten and Kras tumors (Figure S13c). The rare tumors that eventually developed after pairwise inactivation of *Nf1*, *Rasa1*, and *Pten* also had strong activation of RAS and PI3K pathways (Figure S8 and S13d). Based on these

analyses, we propose that these tumors represent a subtype of oncogene-negative lung adenocarcinomas with activated RAS and PI3K pathways (Onc-negative$^{RAS/PI3K}$ subtype).

Oncogene-negative human lung adenocarcinomas frequently have activation of RAS and PI3K pathways

To investigate the activation of RAS and PI3K pathways in human oncogene-negative lung adenocarcinomas, we analyzed oncogene-negative (N=35) and oncogene-positive (N=18) lung adenocarcinomas. Immunohistochemistry for pERK and pAKT showed that ~45% of oncogene-negative human tumors had moderate to strong activation of both RAS and PI3K pathways and thus represent the Onc-negative$^{RAS/PI3K}$ subtype (Figure 4d–h, S13e–j). Activation of the RAS and PI3K pathways were rarely explained by mutations in *NF1*, *PTEN*, or other genes profiled by Stanford's Solid Tumor Actionable Mutation Panel (STAMP; Table S5 and S6), likely due to the noncomprehensiveness of this gene panel, as well as epigenetic mechanisms of RAS and PI3K pathway activation (66). Epigenetic silencing and other non-genomic mechanisms have been well documented to inhibit tumor suppressor genes including *PTEN* (19, 20, 67, 68) . Therefore, we performed immunohistochemistry for PTEN on 20 oncogene-negative lung adenocarcinomas that did not have genomic *PTEN* mutations. Consistent with previous reports, we observed low PTEN protein levels in 13 out of 20 of these tumors (Figure S14a–f) (19).

To assess a larger set of oncogene-negative lung adenocarcinomas for alterations that could lead to the activation of RAS and PI3K pathways, we analyzed oncogene-negative tumors in TCGA and GENIE datasets. We queried a set of well-established negative regulators of the RAS and PI3K pathways for alterations in oncogene-negative tumors (Table S6). Consistent with previous reports, *NF1* and *RASA1* alterations were enriched in oncogene-negative tumors; however, coincident genomic alterations in *NF1*, *RASA1*, and *PTEN* were rare (Figure S14g–h) (69, 70). Importantly, over 60% of oncogene-negative lung adenocarcinomas in TCGA had alterations in either the RAS or PI3K pathways, and 22% of these tumors had alterations in components of both pathways, likely representing Onc-negative$^{RAS/PI3K}$ lung adenocarcinomas (Figure 4i). These frequencies were lower in the GENIE dataset, possibly because only a fraction of the known genes in these pathways were analyzed (Figure S14i). These histological and genomic analyses support a model in which activation of the RAS and PI3K pathways in Onc-negative$^{RAS/PI3K}$ tumors can be generated by diverse genomic and/or epigenetic alterations.

Finally, we assessed whether Onc-negative$^{RAS/PI3K}$ tumors in our mouse model more broadly exhibit transcriptional features that are consistent oncogene-negative human lung adenocarcinoma. We generated a gene expression signature of genes that are higher in Nf1/Rasa1/Pten tumors relative to Kras tumors in mice. We then calculated gene signature activity scores for each TCGA lung adenocarcinoma for this Onc-negative$^{RAS/PI3K}$ gene expression signature using single-sample GSEA (Table S4). Interestingly, the Onc-negative$^{RAS/PI3K}$ signature was highest in oncogene-negative human lung adenocarcinomas relative to lung adenocarcinomas driven by oncogenic *KRAS* or other known oncogenes (Figure 4j). Collectively, these data indicate that the molecular and biochemical state of

mouse Onc-negative$^{RAS/PI3K}$ tumors recapitulates that of a substantial fraction of oncogene-negative human lung adenocarcinomas.

Onc-negative$^{RAS/PI3K}$ tumors are vulnerable to inhibition of RAS and PI3K-AKT pathways

Understanding the biochemical changes that drive tumor development can nominate potential therapeutic strategies (55). To investigate the therapeutic impact of targeting key nodes in Onc-negative$^{RAS/PI3K}$ lung cancer, we initiated tumors in *TC* mice with a pool of barcoded sgRNA viral vectors targeting *Nf1*, *Rasa1*, and *Pten*. We treated these mice with the SHP2 inhibitor RMC-4550 (39), AKT1/2 inhibitor capivasertib (71, 72), or a combination of the two (Figure 5a and S15a–b). These drugs were chosen based on their ongoing clinical development and ability to reduce activation RAS and PI3K pathways (39, 72).

Direct fluorescence imaging and histology indicated that SHP2 inhibition and combined SHP2 and AKT1/2 inhibition greatly reduced tumor burden (Figure 5b–c and S15c). Tuba-seq analysis provided insight into the overall and genotype-specific responses of tumors to the therapeutic interventions. Capivasertib monotherapy was ineffective *in vivo* while RMC-4550 reduced the total tumor burden. The combination of RMC-4550 and capivasertib trended towards being the most efficient therapeutic approach reducing tumor burden by ~30% compared with RMC-4550 alone (Figure 5d, S15d–g).

We confirmed the inhibition of RAS and PI3K pathways in Onc-negative$^{RAS/PI3K}$ tumors in mice treated with RMC-4550 and capivasertib (Figure S15h). Furthermore, global gene expression analysis confirmed the downregulation of RAS and PI3K-AKT gene expression signatures after coincident SHP2 and AKT1/2 inhibition (Figure S16a–d). Treated tumors tended to have higher expression of an apoptosis gene expression signature and lower expression of a G2/M gene expression signature, suggesting that this combination induces broad cellular changes (Figure S16e–f).

Inhibition of SHP2 and AKT synergizes to reduce the growth of Onc-negative$^{RAS/PI3K}$ lung adenocarcinoma cell lines

To more extensively characterize the responses to SHP2 and AKT inhibition, we generated *Nf1/Rasa1/Pten* deficient Onc-negative$^{RAS/PI3K}$ cell lines from tumors initiated with Lenti-sg*Nf1*-sg*Rasa1*-sg*Pten*/*Cre* in *Trp53*$^{flox/flox}$;*TC* mice (Figure 6a and S17a, b). As anticipated, RAS and PI3K signaling was reduced in response to treatment with RMC-4550 and capivasertib, respectively (Figure S17c). RMC-4550 and capivasertib each decreased the overall growth of Onc-negative$^{RAS/PI3K}$ cell lines in a dose-dependent manner (Figure 6b and S17d, e). Consistent with our *in vivo* observations, RMC-4550 and capivasertib synergized to inhibit the growth of these cell lines (Figure 6c and S17f, g). RMC-4550 and capivasertib inhibited proliferation and induced apoptosis to a greater extent than RMC-4550 or capivasertib alone (Figure 6d–e). RMC-4550 and capivasertib treatment also leads to regression of subcutaneous allografts generated from these Onc-negative$^{RAS/PI3K}$ cell lines (Figure 6f–g and S17h–j).

Building on these findings, we assessed activation of RAS and PI3K pathways and driver pathway vulnerabilities in two oncogene-negative human lung adenocarcinoma cell lines,

NCI-H1838 (*NF1*^{LOF}) and NCI-H1623 (*RASA1*^{LOF}). H1838 and H1623 had activation of RAS and PI3K pathways (Figure S17k). Consistent with our findings in mouse Onc-negative$^{RAS/PI3K}$ cell lines, RMC-4550 synergizes with capivasertib to inhibit the growth of these human Onc-negative$^{RAS/PI3K}$ lung adenocarcinoma cell lines (Figure 6h–i and S17l–m). These *in vivo* and cell culture analyses indicate that Onc-negative$^{RAS/PI3K}$ tumors are vulnerable to therapeutic inhibition of these pathways.

DISCUSSION

It is often overlooked that lung adenocarcinomas without genomic alterations in oncogenes afflict as many patients as those driven by either oncogenic KRAS or EGFR. By querying an extensive set of tumor suppressor gene alterations, we uncovered combinatorial tumor suppressor inactivation as a driver of oncogene-negative lung adenocarcinomas. Importantly, combinatorial inactivation of negative regulators of RAS and PI3K pathways are as potent as oncogenic KRAS^{G12D} in initiating lung tumors *in vivo*.

Furthermore, while *NF1* inactivation is sometimes suggested to be an “oncogenic driver” in lung adenocarcinoma (4, 51, 73), *Nf1* inactivation alone is insufficient to initiate lung tumors (Figure S8). Even pairwise inactivation of *Nf1* and *Rasa1*, as well as many other tumor suppressor genes, generated very few tumors even after long time periods (Figure S8). These data suggest that genomic and/or epigenetic alterations in multiple genes within and across pathways may be required to surpass the thresholds necessary for Onc-negative$^{RAS/PI3K}$ lung adenocarcinoma initiation and growth.

Although cancers harbor diverse genomic and epigenomic alterations, these alterations often converge on key pathways and generate similar biochemical changes (12, 74). Pathway activation through genomic and epigenomic inactivation of tumor suppressors can be very diverse, precluding the identification of non-oncogene drivers from gene-centric analysis of human cancer genomic data. Notably, our pathway analysis in oncogene-negative lung adenocarcinomas indicated that mutations in different genes that converge on the RAS and PI3K pathways frequently co-occur (Figure 4i and S14i). Furthermore, previous reports and our observations suggest frequent non-genomic mechanisms of downregulation of RAS GAPs and PTEN (Figure 4f–h, S14a–f) (4, 19–21, 67, 68). Thus, genomic alterations should be viewed as a floor, not a ceiling, in estimating the frequency of pathway alteration.

We assessed the ability of hundreds of complex tumor suppressor genotypes to generate lung tumors. While activation of RAS and PI3K pathway emerged as the most potent driver of oncogene-negative lung adenocarcinomas, our data also suggest that combinatorial inactivation of tumor suppressor genes outside these two pathways can likely initiate tumorigenesis (Figure 2 and S6). Given the mutational diversity and complexity of oncogene-negative human lung adenocarcinomas (75), there remain many other mutational combinations to be investigated. We anticipate that additional studies will uncover other oncogene negative tumor subtypes beyond Onc-negative$^{RAS/PI3K}$ lung adenocarcinomas.

Knowledge of the genes underlying human cancer is a pillar of cancer diagnostics, personalized medicine, and the selection of rational combination therapies. Our data

demonstrate RAS and PI3K pathway activation in the absence of oncogene mutations in a sizable fraction of human lung adenocarcinoma that could predict therapeutic vulnerability to SHP2 and AKT inhibitors. Beyond SHP2 and AKT, extensive efforts have generated inhibitors for many other components of the RAS and PI3K pathways. Thus, further investigation of the therapeutic targeting of key nodes within the RAS pathway (*e.g.*, SOS, MEK, ERK) and PI3K pathway (*e.g.*, PI3K, mTOR), could contribute to the development of the most effective therapies for Onc-negative$^{RAS/PI3K}$ lung adenocarcinomas.

Our findings uncover tumorigenic mechanisms and clinical features of oncogene-negative lung adenocarcinomas. This work identifies biomarkers and new therapeutic targets for Onc-negative$^{RAS/PI3K}$ tumors. The generation of comprehensive molecular and pharmacogenomic maps of oncogene-negative lung adenocarcinomas will transform our understanding of these heretofore poorly characterized lung cancer subtypes.

Supplementary Material

Refer to Web version on PubMed Central for supplementary material.

ACKNOWLEDGEMENTS

We thank the Stanford Shared FACS Facility, Stanford Veterinary Animal Care Staff, Human Pathology/Histology Service Center, and Stanford Protein and Nucleic Acid Facility; A. Orantes and S. Mello for administrative support; Stanford's Molecular Genetic Pathology Laboratory and Henning Stehr for help in providing genetically profiled tumor tissues. David Feldser, Joseph Lipsick, Eric Collisson, Christopher McFarland, and members of the Winslow and Petrov laboratories for helpful discussions and reviewing the manuscript. We thank Florent Elefteriou and Alejandro Sweet-Cordero for providing mouse strains. M. Yousefi was supported by a Stanford University School of Medicine Dean's fellowship, an American Lung Association grant, and an NIH Ruth L. Kirschstein National Research Service Award (F32-CA236311). G. Boross, H. Cai, and J.D. Hebert were supported by Tobacco-Related Disease Research Program Postdoctoral Fellowships (T31FT-1772, 28FT-0019, and T31FT-1619). C.W.M. was supported by the NSF Graduate Research Fellowship Program and an Anne T. and Robert M. Bass Stanford Graduate Fellowship. W-Y. Lin was supported by an AACR Postdoctoral fellowship (17-40-18-LIN). C. Li was the Connie and Bob Lurie Fellow of the Damon Runyon Cancer Research Foundation (DRG-2331). E.L. Ashkin and C.I. Colón were supported by PHS Grant Number CA09302. E.L. Ashkin was also supported by HHMI Gilliam Fellowship for Advanced Study (GT14928). This work was supported by NIH R01-CA231253 (to M.M. Winslow and D.A. Petrov), NIH R01-CA230919 (to M.M. Winslow) and NIH R01-CA234349 (to M.M. Winslow and D.A. Petrov), as well as by the Stanford Cancer Institute, an NCI-designated Comprehensive Cancer Center.

CONFLICT OF INTERESTS

S.K.C. receives grant support from Ono Pharma. C.S. acknowledges grant support from Pfizer, AstraZeneca, Bristol Myers Squibb, Roche-Ventana, Boehringer-Ingelheim, Archer Dx, and Ono Pharmaceuticals. C.S is an AstraZeneca Advisory Board member and Chief Investigator for the MeRmaiD1 clinical trial, has consulted for Pfizer, Novartis, GlaxoSmithKline, MSD, Bristol Myers Squibb, Celgene, AstraZeneca, Illumina, Amgen, Genentech, Roche-Ventana, GRAIL, Medicxi, Bicycle Therapeutics, and the Sarah Cannon Research Institute, has stock options in Apogen Biotechnologies, Epic Bioscience, GRAIL, and has stock options and is co-founder of Achilles Therapeutics. D.A.P. and M.M.W. are founders of, and hold equity in, D2G Oncology Inc.

References:

1. Barta JA, Powell CA, Wisnivesky JP, Global Epidemiology of Lung Cancer. Ann Glob Health 85, (2019).
2. Devarakonda S, Morgensztern D, Govindan R, Genomic alterations in lung adenocarcinoma. Lancet Oncol 16, e342–351 (2015). [PubMed: 26149886]
3. McDermott U, Downing JR, Stratton MR, Genomics and the continuum of cancer care. N Engl J Med 364, 340–350 (2011). [PubMed: 21268726]

4. N. Cancer Genome Atlas Research, Comprehensive molecular profiling of lung adenocarcinoma. Nature 511, 543–550 (2014). [PubMed: 25079552]
5. Carrot-Zhang J et al. , Whole-genome characterization of lung adenocarcinomas lacking the RTK/RAS/RAF pathway. Cell Rep 34, 108707 (2021). [PubMed: 33535033]
6. Campbell JD et al. , Distinct patterns of somatic genome alterations in lung adenocarcinomas and squamous cell carcinomas. Nat Genet 48, 607–616 (2016). [PubMed: 27158780]
7. Vaishnavi A et al. , Oncogenic and drug-sensitive NTRK1 rearrangements in lung cancer. Nat Med 19, 1469–1472 (2013). [PubMed: 24162815]
8. Jonna S et al. , Detection of NRG1 Gene Fusions in Solid Tumors. Clin Cancer Res 25, 4966–4972 (2019). [PubMed: 30988082]
9. Takeuchi K et al. , RET, ROS1 and ALK fusions in lung cancer. Nat Med 18, 378–381 (2012). [PubMed: 22327623]
10. Izumi H et al. , The CLIP1-LTK fusion is an oncogenic driver in non-small-cell lung cancer. Nature, (2021).
11. Vogelstein B et al. , Cancer genome landscapes. Science 339, 1546–1558 (2013). [PubMed: 23539594]
12. Sanchez-Vega F et al. , Oncogenic Signaling Pathways in The Cancer Genome Atlas. Cell 173, 321–337 e310 (2018). [PubMed: 29625050]
13. Krogan NJ, Lippman S, Agard DA, Ashworth A, Ideker T, The cancer cell map initiative: defining the hallmark networks of cancer. Mol Cell 58, 690–698 (2015). [PubMed: 26000852]
14. George J et al. , Comprehensive genomic profiles of small cell lung cancer. Nature 524, 47–53 (2015). [PubMed: 26168399]
15. Gouyer V et al. , Mechanism of retinoblastoma gene inactivation in the spectrum of neuroendocrine lung tumors. Am J Respir Cell Mol Biol 18, 188–196 (1998). [PubMed: 9476905]
16. Sekido Y, Fong KM, Minna JD, Molecular genetics of lung cancer. Annu Rev Med 54, 73–87 (2003). [PubMed: 12471176]
17. Meuwissen R et al. , Induction of small cell lung cancer by somatic inactivation of both Trp53 and Rb1 in a conditional mouse model. Cancer Cell 4, 181–189 (2003). [PubMed: 14522252]
18. Govindan R et al. , Genomic landscape of non-small cell lung cancer in smokers and never-smokers. Cell 150, 1121–1134 (2012). [PubMed: 22980976]
19. Soria JC et al. , Lack of PTEN expression in non-small cell lung cancer could be related to promoter methylation. Clin Cancer Res 8, 1178–1184 (2002). [PubMed: 12006535]
20. Kazanets A, Shorstova T, Hilmi K, Marques M, Witcher M, Epigenetic silencing of tumor suppressor genes: Paradigms, puzzles, and potential. Biochim Biophys Acta 1865, 275–288 (2016). [PubMed: 27085853]
21. Ding L et al. , Somatic mutations affect key pathways in lung adenocarcinoma. Nature 455, 1069–1075 (2008). [PubMed: 18948947]
22. Lee JS, Grisham JW, Thorgeirsson SS, Comparative functional genomics for identifying models of human cancer. Carcinogenesis 26, 1013–1020 (2005). [PubMed: 15677630]
23. Gao Q et al. , Driver Fusions and Their Implications in the Development and Treatment of Human Cancers. Cell Rep 23, 227–238 e223 (2018). [PubMed: 29617662]
24. Lu X et al. , MET Exon 14 Mutation Encodes an Actionable Therapeutic Target in Lung Adenocarcinoma. Cancer Res 77, 4498–4505 (2017). [PubMed: 28522754]
25. Liu J et al. , An Integrated TCGA Pan-Cancer Clinical Data Resource to Drive High-Quality Survival Outcome Analytics. Cell 173, 400–416 e411 (2018). [PubMed: 29625055]
26. Liu C et al. , Mosaic analysis with double markers reveals tumor cell of origin in glioma. Cell 146, 209–221 (2011). [PubMed: 21737130]
27. Zhu Y et al. , Ablation of NF1 function in neurons induces abnormal development of cerebral cortex and reactive gliosis in the brain. Genes Dev 15, 859–876 (2001). [PubMed: 11297510]
28. Jackson EL et al. , Analysis of lung tumor initiation and progression using conditional expression of oncogenic K-ras. Genes Dev 15, 3243–3248 (2001). [PubMed: 11751630]
29. Madisen L et al. , A robust and high-throughput Cre reporting and characterization system for the whole mouse brain. Nat Neurosci 13, 133–140 (2010). [PubMed: 20023653]

30. Chiou SH et al. , Pancreatic cancer modeling using retrograde viral vector delivery and in vivo CRISPR/Cas9-mediated somatic genome editing. Genes Dev 29, 1576–1585 (2015). [PubMed: 26178787]
31. Okawa H et al. , Hepatocyte-specific deletion of the keap1 gene activates Nrf2 and confers potent resistance against acute drug toxicity. Biochem Biophys Res Commun 339, 79–88 (2006). [PubMed: 16293230]
32. Bardeesy N et al. , Loss of the Lkb1 tumour suppressor provokes intestinal polyposis but resistance to transformation. Nature 419, 162–167 (2002). [PubMed: 12226664]
33. Jonkers J et al. , Synergistic tumor suppressor activity of BRCA2 and p53 in a conditional mouse model for breast cancer. Nat Genet 29, 418–425 (2001). [PubMed: 11694875]
34. Rogers ZN et al. , A quantitative and multiplexed approach to uncover the fitness landscape of tumor suppression in vivo. Nat Methods 14, 737–742 (2017). [PubMed: 28530655]
35. Cai H et al. , A Functional Taxonomy of Tumor Suppression in Oncogenic KRAS-Driven Lung Cancer. Cancer Discov 11, 1754–1773 (2021). [PubMed: 33608386]
36. Rogers ZN et al. , Mapping the in vivo fitness landscape of lung adenocarcinoma tumor suppression in mice. Nat Genet 50, 483–486 (2018). [PubMed: 29610476]
37. Fedchenko N, Reifenrath J, Different approaches for interpretation and reporting of immunohistochemistry analysis results in the bone tissue - a review. Diagn Pathol 9, 221 (2014). [PubMed: 25432701]
38. Feoktistova M, Geserick P, Leverkus M, Crystal Violet Assay for Determining Viability of Cultured Cells. Cold Spring Harb Protoc 2016, pdb prot087379 (2016).
39. Nichols RJ et al. , RAS nucleotide cycling underlies the SHP2 phosphatase dependence of mutant BRAF-, NF1- and RAS-driven cancers. Nat Cell Biol 20, 1064–1073 (2018). [PubMed: 30104724]
40. Ianevski A, Giri AK, Aittokallio T, SynergyFinder 2.0: visual analytics of multi-drug combination synergies. Nucleic Acids Res 48, W488–W493 (2020). [PubMed: 32246720]
41. Loewe S, The problem of synergism and antagonism of combined drugs. Arzneimittelforschung 3, 285–290 (1953). [PubMed: 13081480]
42. Dobin A et al. , STAR: ultrafast universal RNA-seq aligner. Bioinformatics 29, 15–21 (2013). [PubMed: 23104886]
43. Li B, Dewey CN, RSEM: accurate transcript quantification from RNA-Seq data with or without a reference genome. BMC Bioinformatics 12, 323 (2011). [PubMed: 21816040]
44. Soneson C, Love MI, Robinson MD, Differential analyses for RNA-seq: transcript-level estimates improve gene-level inferences. F1000Res 4, 1521 (2015). [PubMed: 26925227]
45. Love MI, Huber W, Anders S, Moderated estimation of fold change and dispersion for RNA-seq data with DESeq2. Genome Biol 15, 550 (2014). [PubMed: 25516281]
46. Subramanian A et al. , Gene set enrichment analysis: a knowledge-based approach for interpreting genome-wide expression profiles. Proc Natl Acad Sci U S A 102, 15545–15550 (2005). [PubMed: 16199517]
47. Hanzelmann S, Castelo R, Guinney J, GSVA: gene set variation analysis for microarray and RNA-seq data. BMC Bioinformatics 14, 7 (2013). [PubMed: 23323831]
48. Hutter C, Zenklusen JC, The Cancer Genome Atlas: Creating Lasting Value beyond Its Data. Cell 173, 283–285 (2018). [PubMed: 29625045]
49. A. P. G. Consortium, AACR Project GENIE: Powering Precision Medicine through an International Consortium. Cancer Discov 7, 818–831 (2017). [PubMed: 28572459]
50. Jorge SE, Kobayashi SS, Costa DB, Epidermal growth factor receptor (EGFR) mutations in lung cancer: preclinical and clinical data. Braz J Med Biol Res 47, 929–939 (2014). [PubMed: 25296354]
51. Skoulidis F, Heymach JV, Co-occurring genomic alterations in non-small-cell lung cancer biology and therapy. Nat Rev Cancer 19, 495–509 (2019). [PubMed: 31406302]
52. Saito M et al. , Gene aberrations for precision medicine against lung adenocarcinoma. Cancer Sci 107, 713–720 (2016). [PubMed: 27027665]

53. Winters IP et al. , Multiplexed in vivo homology-directed repair and tumor barcoding enables parallel quantification of Kras variant oncogenicity. Nat Commun 8, 2053 (2017). [PubMed: 29233960]
54. Winters IP, Murray CW, Winslow MM, Towards quantitative and multiplexed in vivo functional cancer genomics. Nat Rev Genet 19, 741–755 (2018). [PubMed: 30267031]
55. Lynch TJ et al. , Activating mutations in the epidermal growth factor receptor underlying responsiveness of non-small-cell lung cancer to gefitinib. N Engl J Med 350, 2129–2139 (2004). [PubMed: 15118073]
56. Ohashi K et al. , Characteristics of lung cancers harboring NRAS mutations. Clin Cancer Res 19, 2584–2591 (2013). [PubMed: 23515407]
57. Lin Q et al. , The association between BRAF mutation class and clinical features in BRAF-mutant Chinese non-small cell lung cancer patients. J Transl Med 17, 298 (2019). [PubMed: 31470866]
58. Paez JG et al. , EGFR mutations in lung cancer: correlation with clinical response to gefitinib therapy. Science 304, 1497–1500 (2004). [PubMed: 15118125]
59. Politi K et al. , Lung adenocarcinomas induced in mice by mutant EGF receptors found in human lung cancers respond to a tyrosine kinase inhibitor or to down-regulation of the receptors. Genes Dev 20, 1496–1510 (2006). [PubMed: 16705038]
60. Li D et al. , Bronchial and peripheral murine lung carcinomas induced by T790M-L858R mutant EGFR respond to HKI-272 and rapamycin combination therapy. Cancer Cell 12, 81–93 (2007). [PubMed: 17613438]
61. van Veen JE et al. , Mutationally-activated PI3'-kinase-alpha promotes de-differentiation of lung tumors initiated by the BRAF(V600E) oncoprotein kinase. Elife 8, (2019).
62. Dankort D et al. , A new mouse model to explore the initiation, progression, and therapy of BRAFV600E-induced lung tumors. Genes Dev 21, 379–384 (2007). [PubMed: 17299132]
63. Winslow MM et al. , Suppression of lung adenocarcinoma progression by Nkx2-1. Nature 473, 101–104 (2011). [PubMed: 21471965]
64. Sweet-Cordero A et al. , An oncogenic KRAS2 expression signature identified by cross-species gene-expression analysis. Nat Genet 37, 48–55 (2005). [PubMed: 15608639]
65. Agarwal A et al. , The AKT/I kappa B kinase pathway promotes angiogenic/metastatic gene expression in colorectal cancer by activating nuclear factor-kappa B and beta-catenin. Oncogene 24, 1021–1031 (2005). [PubMed: 15592509]
66. Yang SR et al. , Comprehensive Genomic Profiling of Malignant Effusions in Patients with Metastatic Lung Adenocarcinoma. J Mol Diagn 20, 184–194 (2018). [PubMed: 29269277]
67. Maertens O, Cichowski K, An expanding role for RAS GTPase activating proteins (RAS GAPs) in cancer. Adv Biol Regul 55, 1–14 (2014). [PubMed: 24814062]
68. Song MS, Salmena L, Pandolfi PP, The functions and regulation of the PTEN tumour suppressor. Nat Rev Mol Cell Biol 13, 283–296 (2012). [PubMed: 22473468]
69. Hayashi T et al. , RASA1 and NF1 are Preferentially Co-Mutated and Define A Distinct Genetic Subset of Smoking-Associated Non-Small Cell Lung Carcinomas Sensitive to MEK Inhibition. Clin Cancer Res 24, 1436–1447 (2018). [PubMed: 29127119]
70. Kitajima S, Barbie DA, RASA1/NF1-Mutant Lung Cancer: Racing to the Clinic? Clin Cancer Res 24, 1243–1245 (2018). [PubMed: 29343556]
71. Middleton G et al. , The National Lung Matrix Trial of personalized therapy in lung cancer. Nature 583, 807–812 (2020). [PubMed: 32669708]
72. Davies BR et al. , Preclinical pharmacology of AZD5363, an inhibitor of AKT: pharmacodynamics, antitumor activity, and correlation of monotherapy activity with genetic background. Mol Cancer Ther 11, 873–887 (2012). [PubMed: 22294718]
73. O'Neill AC, Jagannathan JP, Ramaiya NH, Evolving Cancer Classification in the Era of Personalized Medicine: A Primer for Radiologists. Korean J Radiol 18, 6–17 (2017). [PubMed: 28096714]
74. Hanahan D, Weinberg RA, Hallmarks of cancer: the next generation. Cell 144, 646–674 (2011). [PubMed: 21376230]

75. Lawrence MS et al. , Mutational heterogeneity in cancer and the search for new cancer-associated genes. Nature 499, 214–218 (2013). [PubMed: 23770567]

Statement of Significance

To address the large fraction of lung adenocarcinomas lacking mutations in proto-oncogenes for which targeted therapies are unavailable, this work uncovers driver pathways of oncogene-negative lung adenocarcinomas and demonstrates their therapeutic vulnerabilities.

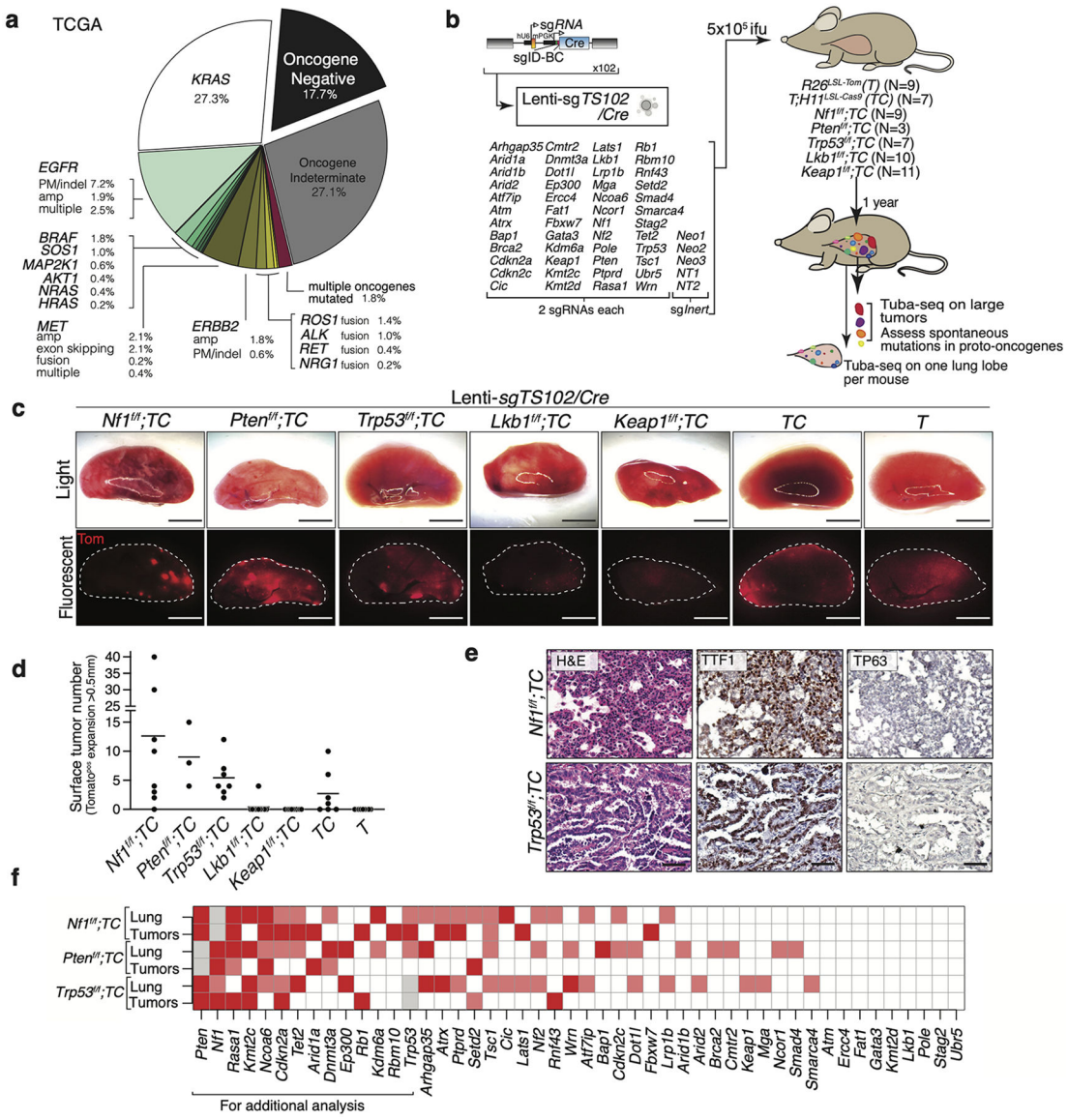

Figure 1. Combinatorial tumor suppressor inactivation enables lung tumor development in the absence of engineered oncogenes.

a. Frequency of oncogene-positive, oncogene-indeterminate, and oncogene-negative human lung adenocarcinomas. Data from TCGA. PM: point mutation, indel: insertion and deletion, amp: amplification, multiple: multiple alterations in the same gene.

b. Combined Cre/lox and CRISPR/Cas9-mediated tumor suppressor gene inactivation to generate lung epithelial cells with diverse genotypes. The number of mice in each group is indicated.

c. Representative light and fluorescence images of lung lobes from the indicated genotypes of mice one year after transduction with the Lenti-sg *TS102/Cre* pool. Lung lobes are outlined with white dotted lines. Scale bar = 4 mm

d. The number of surface tumors (defined as Tomato-positive expansions greater than 0.5 mm in diameter) quantified by direct counting. Each dot represents a mouse, and the bar is the mean.

e. Representative Hematoxylin and Eosin (H&E), TTF1, and TP63 stained sections of the indicated genotypes of mice. Scale bar = 100 μm

f. Heatmap showing two measures of tumor suppressor strengths in each genotype detected using Tuba-seq analysis: “Tumors” is the occurrence of tumor suppressor gene targeting vectors in dissected tumors. $p < 0.001$ (red), $p < 0.1$ (pink) (see Figure S4). “Lung” represents the increase in median sizes of clonal expansions in bulk lung lobe samples. Significant increases ($p<0.05$) in sizes of clonal expansions with all sgRNAs (red) and those with only one significant sgRNA (pink) (see Figure S5). Gray boxes indicate redundant targeting of genes by both Cre/*loxP* and CRISPR/Cas9.

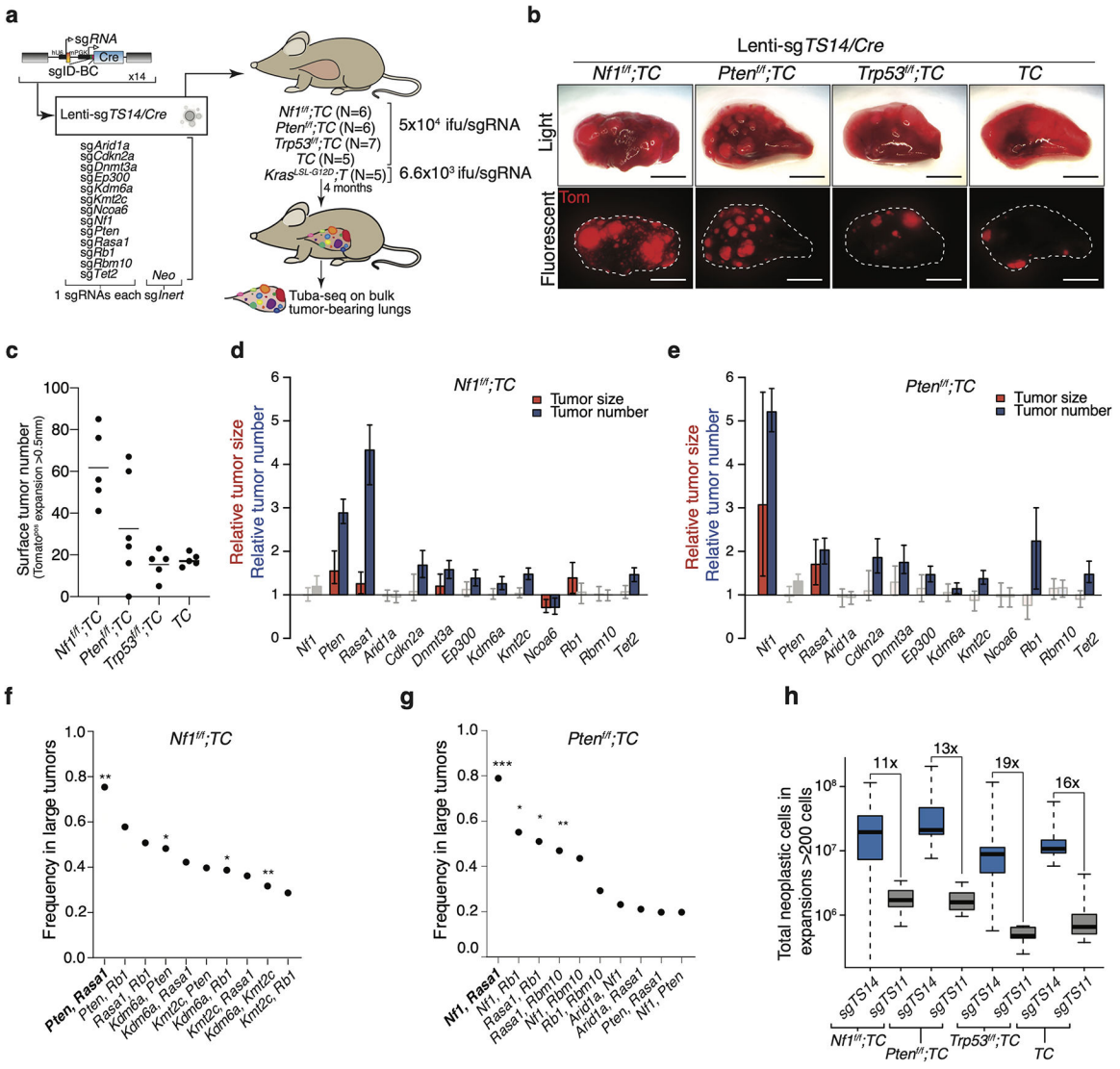

Figure 2. *Nf1*, *Rasa1*, and *Pten* emerge as key drivers of oncogene-negative lung adenocarcinoma.

a. Combined Cre/lox and CRISPR/Cas9-mediated tumor suppressor gene inactivation to generate lung epithelial cells with diverse genotypes. The number of mice in each group is indicated.

b. Representative light and fluorescence images of lung lobes from the indicated genotypes of mice. Lung lobes are outlined with white dotted lines. Scale bar = 4mm

c. The number of tumors (defined as Tomato-positive expnsions larger than 0.5 mm in diameter) quantified by direct counting. Each dot represents a mouse and the bar is the mean.

d,e. The number of tumors with a minimum size of 1000 neoplastic cells, relative to inert sgRNA containing expansions are shown as blue bars. 90th percentile of tumor sizes relative to inert sgRNAs are shown as red bars. sgRNAs that significantly impact tumor number or size ($p<0.05$) are in darker colors. Whiskers show 95% confidence intervals.

f,g. Barcodes with the highest counts in each mouse were investigated for coinfection with multiple Lenti-sg*TS/Cre* vectors (*i.e.*, tumors initiated from cells transduced with multiple

viruses, which result in complex tumor suppressor genotypes, see Methods). The most frequently co-mutated pairs of tumor suppressor genes are shown. Combinations of sgRNAs that lead to the generation of *Nf1*, *Rasa1*, and *Pten* mutant cancer cells are in bold. *p<0.05, **p<0.01, ***p<0.001 based on a permutation test.

h. Total number of neoplastic cells in clonal expansions with more than 200 cells in the indicated genotypes of mice after receiving Lenti-*sgTS14/Cre* or Lenti-*sgTS11/Cre* (which lacks lentiviral vectors containing sg*Nf1*, sg*Rasa1*, and sg*Pten*). The magnitude of reduction in neoplastic cell number is indicated.

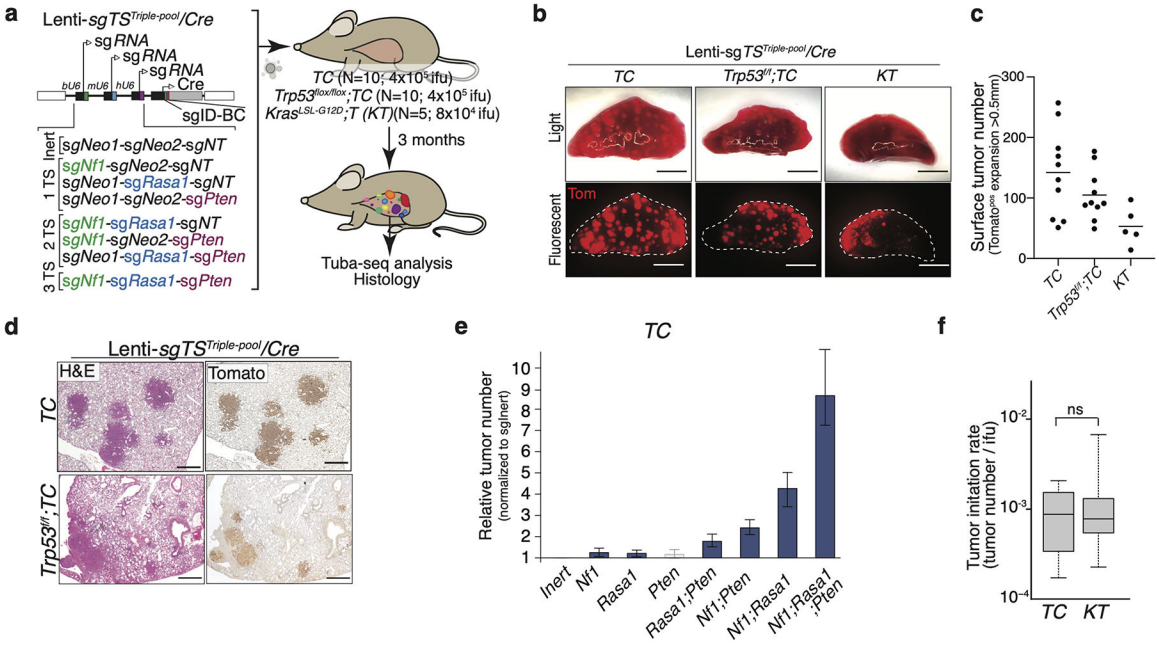

Figure 3. Inactivation of *Nf1*, *Rasa1*, and *Pten* allows a stepwise acquisition of growth advantage during lung adenocarcinoma development.

a. Barcoded triple sgRNA vectors for CRISPR/Cas9-mediated inactivation of all combinations of *Nf1*, *Rasa1*, and *Pten* in *TC* and *Trp53flox/flox;TC* mice. sg*Neo1* and sg*Neo2* are active cutting, but inert sgRNAs. *sgNT* is a non-targeting inert sgRNA. Mouse genotype, mouse number, and titers of virus are indicated. Tuba-seq was performed on tumor-bearing lungs 3 months after tumor initiation.

b. Bright-field and fluorescence images of lungs from the indicated mouse genotypes. Lung lobes are outlined with a dashed white line. Scale bar = 4 mm

c. The number of surface tumors (defined as Tomato-positive expansions larger than 0.5 mm in diameter) quantified by direct counting. Each dot represents a mouse and the bar is the mean.

d. Representative H&E and Tomato stained sections of lungs from *TC* and *Trp53flox/flox;TC* mice 3 months after transduction with Lenti-sg*TSTriple-pool/Cre*. Scale bar = 500 μm

e. Numbers of tumors (with >1000 neoplastic cells) relative to the Inert sgRNA containing expansions. sgRNAs resulting in a significantly higher number of tumors than the inert vector ($p<0.05$) are shown in a darker color. Mean +/− 95% confidence interval is shown.

f. Quantification of the ability of combined *Nf1/Rasa1/Pten* inactivation in *TC* mice and oncogenic *KrasG12D* in *KT* mice to initiate tumors. The number of tumors (with >1000 neoplastic cells) per infectious unit (ifu) is shown. The bar is the median, the box represents the interquartile range, and the whiskers show minimum and maximum values. ns: non-significant

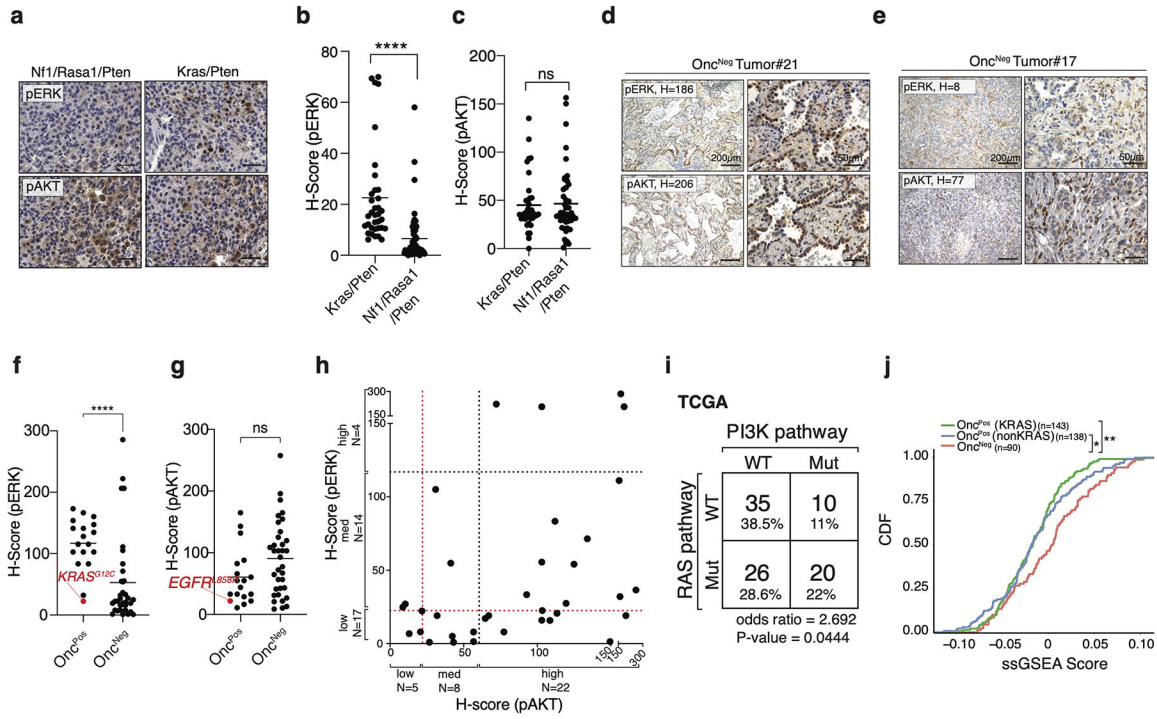

Figure 4. Oncogene-negative mouse and human lung adenocarcinomas have frequent activation of RAS and PI3K pathways.

a-c. Representative immunohistochemistry for pERK and pAKT on tumors with the indicated genotypes and quantification of these stainings. The bar is the mean. n.s: non-significant, ****<p<0.0001 using Mann–Whitney U test. Scale bars= 50μm

d,e. Representative immunohistochemistry for pAKT and pERK on oncogene-negative human tumors. H-scores for the whole section are indicated for each representative image. Scale bar= 200 μM (right), 50 μm (left)

f, g. Quantification of pAKT and pERK staining on 35 oncogene-negative and 18 oncogene-positive human lung adenocarcinomas. Genotypes of oncogene- positive tumors with the lowest pERK and pAKT staining intensities are in red. Significance between groups, Mann-Whitney U test, ns: non-significant, ****p<0.0001

h. pERK and pAKT H-scores for oncogene-negative human tumors replotted from Figure 4f,g. Red dotted lines: the thresholds for low versus medium pERK and pAKT based on the lowest pERK and pATK staining intensity of oncogene-positive lung adenocarcinomas. Black dotted lines: the thresholds for medium versus high pERK and pAKT staining based on the mean pERK and pAKT H-scores in oncogene-positive tumors. The number of tumors in each staining intensity group (low, medium, high) is indicated.

i. Alteration frequency of established components of RAS and PI3K pathways (see Table S6) and their co-occurrences in TCGA data sets. p-value calculated by two-sided Fisher's Exact Test.

j. Cumulative distribution function (CDF) plot of the signature scores for human tumors stratified by genes upregulated in mouse oncogene-negative tumors generated by inactivation of *Nf1*, *Rasa1*, and *Pten* (Figure S14a and see Table S4). Cohort size and P-value calculated by Kolmogorov–Smirnov test are indicated.

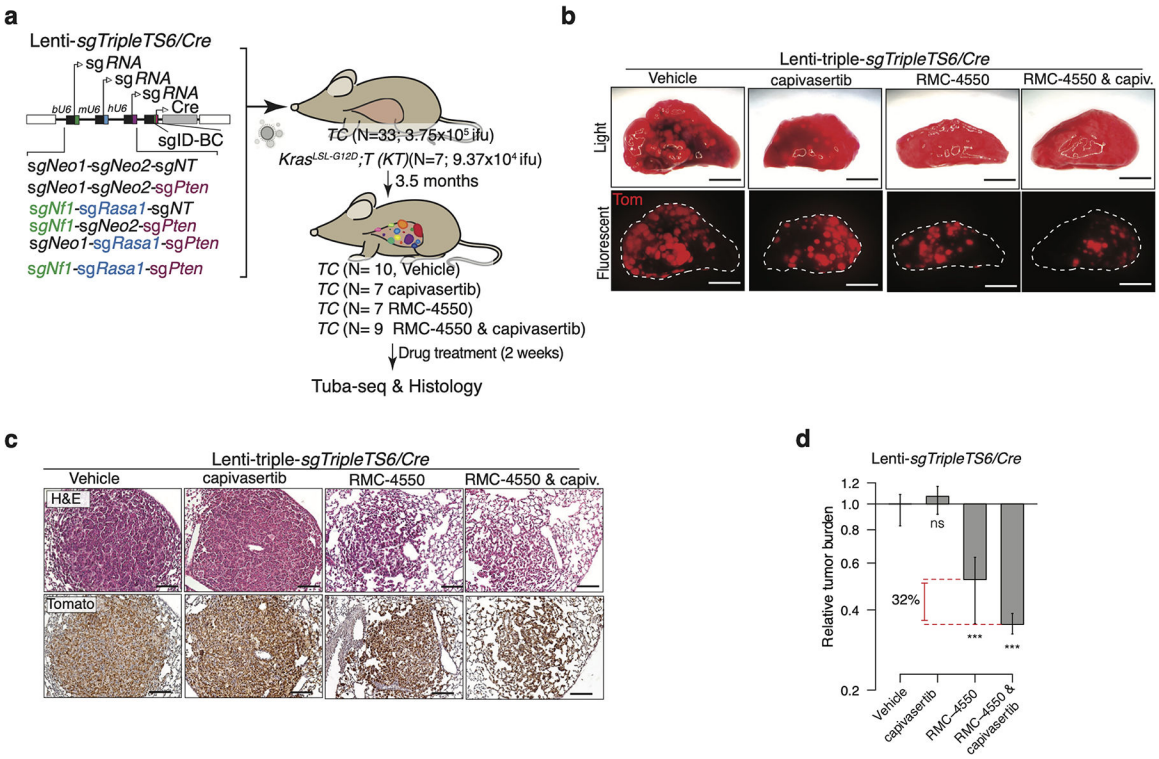

Figure 5. SHP2 and AKT inhibition synergize to reduce the growth of autochthonous oncogene-negative lung tumors.

a. Barcoded triple sgRNA vectors for CRISPR/Cas9-mediated inactivation of combinations of *Nf1*, *Rasa1*, and *Pten* in *TC* mice. Indicated numbers of mice were treated with RMC-4550 (SHP2 inhibitor), capivasertib (AKT inhibitor), or a combination of these two drugs for two weeks 3.5 months after tumor initiation. Tuba-seq and histological analysis were performed on tumor-bearing lungs.

b. Bright-field and fluorescence images of lungs from the indicated mice. Lung lobes are outlined with a dashed white line. Scale bars = 4 mm

c. Representative H&E and Tomato-stained sections of tumors from *TC* mice 3.5 months after transduction with Lenti-sg*TripleTS6/Cre* and two weeks after treatment with the indicated drugs. Scale bars = 100 μm

d. Relative tumor burden after treatment with capivasertib, RMC-4550, and combination of these drugs compared with tumor burden in vehicle-treated mice. ns: non-significant, ***p< 0.001. Drug response is shown for all the tumors.

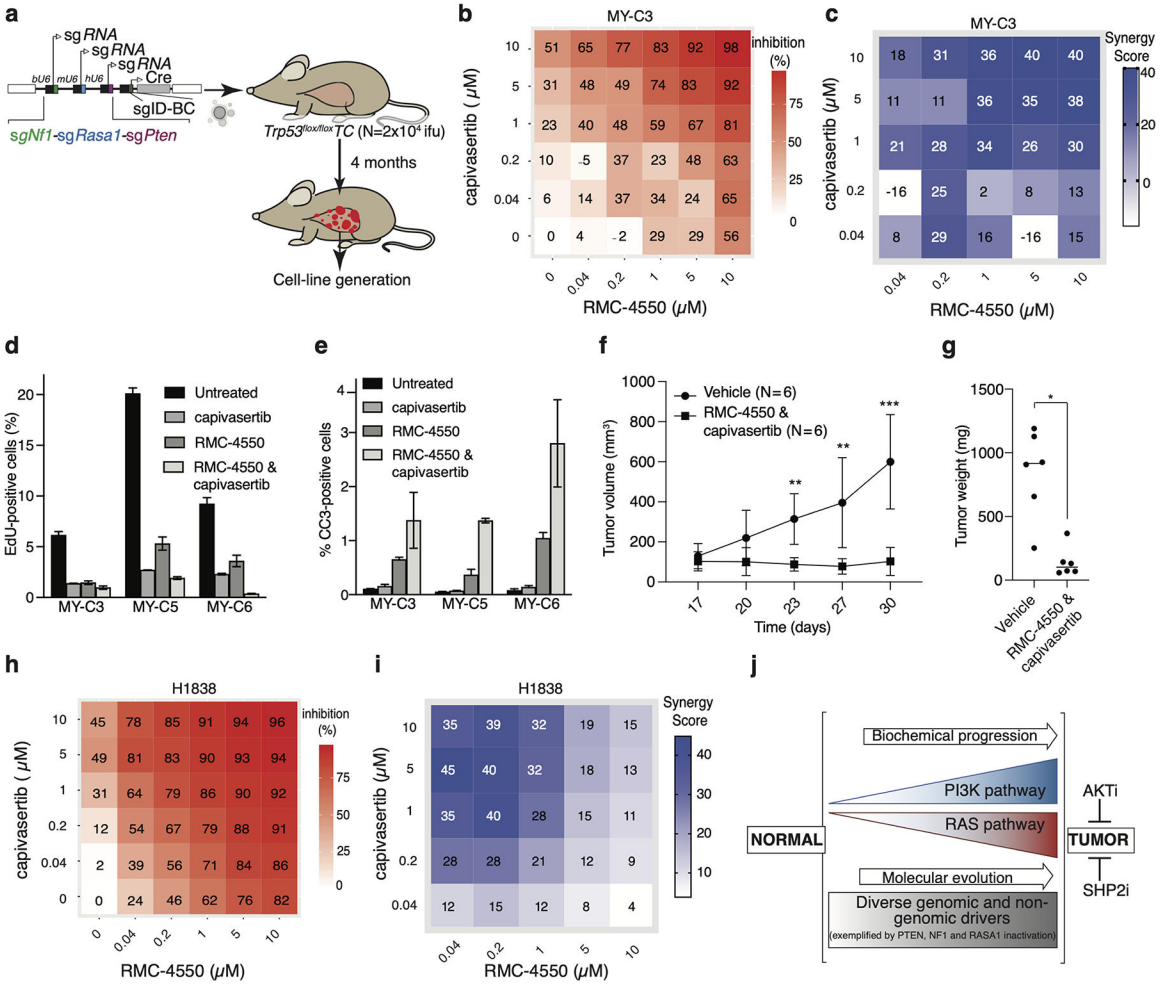

Figure 6. RMC-4550 and capivasertib synergize to inhibit the growth of Onc-negative$^{RAS/PI3K}$ lung adenocarcinoma cell lines.

a. Cell line generation from Onc-negative$^{RAS/PI3K}$ tumors from *Trp53$^{flox/flox}$;TC* mice.

b. Drug dose-response matrix depicting percent growth inhibition of a murine Onc-negativeRAS/PI3K cell line after four days of treatment with the indicated doses of RMC-4550 and capivasertib. The average responses of three to four replicates are shown for each treatment.

c. Loewe's synergy score calculated based on drug responses in Figure 6b. Synergy scores indicate the percentage of response beyond expectation.

d,e. Cell proliferation and apoptosis analysis using EdU incorporation, cleaved caspase 3 staining, and flow-cytometry analysis. Three independent Onc-negativeRAS/PI3K murine cell lines were treated with 10 μM of the indicated drug(s) for 2 days before the analysis.

f. Volumes of cell-line derived allografts from a murine Onc-negative$^{RAS/PI3K}$ cell lines (MY-C3). 17 days after subcutaneous transplantation, 3 mice were treated with vehicle and 3 mice received RMC-4550 and capivasertib.**p<0.001, ***p<0.0001

g. Weights of subcutaneous tumors at the endpoint of the experiment. *p<0.05

h. Drug dose-response matrix depicting percent growth inhibition of H1838, a human Onc-negativeRAS/PI3K lung adenocarcinoma cell line.

i. Loewe's synergy score calculated based on drug responses in Figure 6h.

j. Model of biochemical progression and molecular drivers of Onc-negativeRAS/PI3K tumors.